Atmospheric CH4 measurement near a landfill using an ICL-based QEPAS sensor with V-T relaxation self-calibration

Atmospheric CH_4 measurement near a landfill using an ICL-based QEPAS sensor with V-T relaxation self-calibration

Hongpeng Wu[1,2], Lei Dong[1,2,*], Xukun Yin[1,2], Angelo Sampaolo[3], Pietro Patimisco[3], Weiguang Ma[1,2], Lei Zhang[1,2], Wangbao Yin[1,2], Liantuan Xiao[1,2], Vincenzo Spagnolo[1,2,3] and Suotang Jia[1,2]

[1)] *State Key Laboratory of Quantum Optics and Quantum Optics Devices, Institute of Laser Spectroscopy, Shanxi University, Taiyuan 030006, China*

[2)] *Collaborative Innovation Center of Extreme Optics, Shanxi University, Taiyuan 030006, China*

[3)] *PolySenSe Lab- Physics Department, Università degli Studi di Bari and Politecnico di Bari, CNR-IFN BARI, Via Amendola 173, Bari 70126, Italy*

Abstract: A quartz-enhanced photoacoustic spectroscopy methane (CH_4) sensor with vibrational to translational (V-T) relaxation self-calibration was realized and tested for atmospheric CH_4 detection near a landfill. To normalize the influence of H_2O vapor on the CH_4 energy relaxation rate, CH_4 and H_2O concentrations were detected simultaneously by means of frequency division multiplexing technique, in which a custom quartz tuning fork was operated in the fundamental and first overtone combined vibration. A continuous wave, thermoelectrically cooled distributed feedback interband cascade laser emitting at 3.3 μm and a near-infrared DFB laser emitting at 1.37 μm were used as the excitation source for CH_4 and H_2O detection, respectively. A theoretical model of V-T relaxation and self-calibration method were

* Corresponding author. Tel: +86 3517097220; fax: +86 3517018927.
E-mail address: donglei@sxu.edu.cn

developed to allow this CH_4 sensor to have a simple setup and small sensor size. Continuous field measurements were carried out near the largest sanitary landfill in Shanxi province, China, to demonstrate the stability and ruggedness of the realized CH_4 sensor.

Keywords: Landfill gas emissions; Quartz-enhanced photoacoustic spectroscopy; Optical gas sensor; Gas V-T relaxation; Combined vibration of quartz tuning fork

1. Introduction

Methane (CH_4) is an odorless, flammable gas with atmospheric concentrations of ~1.8 ppm [1, 2]. It is mainly released into the atmosphere by human activities such as leakage from natural gas systems, as well as emission from livestock and landfill. It can also be found in sewers, wetlands and mines. CH_4 has a long lifetime (~ 12 years) and is a highly potent greenhouse gas, ~ 28 times greater warming effect than CO_2 [3]. Highly sensitive and precise measurements of CH_4 are mandatory to monitor its induced global warming and climate change, considering its environmental relevance. According to the United States Environmental Protection Agency, municipal solid waste (MSW) landfills are the third largest source of CH_4 emission [4]. Economic development and rising standards of living lead to increase in the quantity of MSW and most of MSW end up at landfills. These result in a huge generation of landfill gases (LFG). The LFG, mostly consisting of CH_4 (55-60% v/v), CO_2 (40-45% v/v) plus other volatile organic carbons and trace components (<1% v/v), are produced when the organic waste in the MSW is broken down by bacteria naturally present in MSW and the soil [3, 4]. At some large landfills, CH_4 in LFG is collected and utilized for the production of electricity and heat.

Many factors lead to the instability of CH_4 generation, collection and emission, such as wind, temperature, atmospheric pressure, MSW organic content, its compaction degree, age, etc. Hence, although professional equipments are installed to collect the LFG, the LFG utilization cannot be carried out effectively at most landfills. The LFG are either flared with risk of producing toxic combustion products or

emitted into atmosphere. Due to the huge potential of LFG using as an energy source, landfill methane is getting more attention from local governments, utilities, environmental organization together with industry and MSW landfill operators. As a result, detecting, monitoring and capturing methane at former and active landfills are a global housekeeping benefit as well as an important alternative energy niche.

Several optical gas sensing techniques have been employed for CH_4 detection [5-10]. Among them, quartz-enhanced photoacoustic spectroscopy (QEPAS) technique [11], a modification of conventional photoacoustic spectroscopy (PAS), has been demonstrated to provide CH_4 detection with fast response times (<1 s). Such a technique is wavelength independent, capable to analyze small gas samples with high accuracy and sensitivity, and does not require the use of any optical detectors [12-14]. In QEPAS sensing, the photoacoustic signal, generated by the absorption of modulated light from the gas sample, is detected by means of a piezoelectric quartz tuning fork (QTF), acting as a sharply resonant acoustic transducer [15-17]. QTFs are characterized by a high-quality factor Q (>10,000 at atmospheric pressure), a high resonant frequency f_0 (up to few tens of kHz) and narrow resonance width (few Hz or less) as well as high immunity to environmental acoustic noise [18,19]. In most of the reported QEPAS-based sensor, the laser beam is focused on to the gas present between the two QTF prongs and in an acoustic micro-resonator (AmR) tube, which acts as an acoustic resonator for the QTF [20]. A 2f wavelength modulation spectroscopy (2f-WMS) technique is typically employed to excite an anti-symmetric mode of the QTF vibration. The laser modulation frequency must accurately match

with the QTF resonance frequency to obtain the highest signal amplitude [21]. However, when exploiting a standard QTF (resonance frequency of ~32,768 kHz), the modulation frequency f of ~16 kHz is comparable to or exceeds the vibrational to translational (V–T) energy transfer rate ($1/\tau$) in slow-relaxing gas species such as CH_4 or CO, thereby violating the condition for PAS that the molecular relaxation rates $1/\tau$ should be much higher than the modulation frequency, i.e. $f \ll 1/\tau$ [22]. As a result, the observed QEPAS signal exhibits a strongly reduced amplitude and dependence on $1/\tau$ compared to a conventional PAS-based sensor.

One way to enhance the CH_4 QEPAS signal amplitude is to employ a custom-made QTF with a low resonance frequency [18, 19], thus reducing the mismatch between the high modulation frequency of the QEPAS sensor and the low molecular relaxation rate of CH_4. By optimizing the prong spacing and the ratio of the prong width W and the square of the prong length L, the fundamental resonance frequency of a custom QTF was reduced down to ~3 kHz, becoming more suitable for the detection of slow-relaxing gas species [18]. Moreover, the large prong spacing of the custom QTF allowed an easy focalization of mid-IR laser beams between the prongs without hitting them. This is helpful considering that the fundamental ν_3 vibration band of CH_4 molecule with the strongest absorption coefficient is located at ~3.3 μm and can be targeted by interband cascade lasers (ICLs).

In practical applications related with CH_4 detection, such as LFG monitoring or atmospheric CH_4 measurement near a landfill, the presence of water vapor is unavoidable. The H_2O molecules act as V-T relaxation process promoter for CH_4,

hence, to provide reliable CH_4 detection data, an accurate measurement of H_2O concentration is also required, even if implementing low frequency QTFs. The introduction of an additional sensing system for accurate H_2O measurement can limit the capability of in-situ CH_4 measurements for QEPAS-based sensor, as the sensor system becomes more complex and bulkier [23]. This issue can be addressed by exploiting the capability of the QTFs to simultaneously operate at different vibrational modes. Indeed, the reduction in the 1st overtone resonance frequency down to 18 kHz achieved with custom QTFs opens the way to the implementation of the overtone flexural mode for QEPAS operation [24]. The overtone vibration mode can be combined with the fundamental vibration mode to realize simultaneous dual-gas QEPAS detection via using the frequency division multiplexing (FDM) technique. Thereby, the additional detection channel could be devoted to monitoring the H_2O vapor concentration and this information can be used to normalize the CH_4 slow-relaxing QEPAS signal amplitude.

In this paper, we reported on the realization of a CH_4 QEPAS sensor based on the simultaneous fundamental and 1st overtone in-plane flexural mode excitation of a custom QTF. The first overtone vibration mode was exploited to detect the CH_4 molecule, while H_2O vapor was monitored using the fundamental vibration mode. By simultaneously measuring both CH_4 and H_2O concentration levels, the H_2O influence on the V-T relaxation of CH_4 molecule can be compensated. The performances of the developed CH_4 / H_2O sensor system with V-T relaxation self-calibration was investigated and optimized. At last, an atmospheric CH_4 measurement near a landfill

was implemented to verify the robustness and reliability of the sensor.

2. Theoretical background

2.1 Theory of QTF flexural vibration modes

It has been confirmed theoretically and experimentally that a QTF can be modeled as a series resistance-inductor-capacitor circuit based on the *RLC* Butterworth-Van Dyke model. The model uses an electrical analogy of a mechanical damped oscillator, in which R represents the acoustic losses in the material (intrinsic losses) and its environment (extrinsic losses), L and $1/C$ represent the mass and the stiffness of the cantilever [18, 19, 25]. For the fundamental flexural mode, the prong can be analyzed as a single point-mass system and the point-mass is located at the prong tip, while for the first overtone flexural mode, the prong can be considered as a system of two-coupled point-mass subsystems. The point-masses are located at the different antinodes [24]. The QTF should be excited at the antinode positions in order to obtain the largest QEPAS signal [26]. When a QTF operates at a combined vibration mode, it can be modeled as two electric equivalents *RLC* circuit connecting in parallel, as shown in Fig. 1(a).

In a QTF, the two prongs are connected through a U-shape base. Differently from a standard cantilever, the center of mass of the QTF remains static when the prongs are vibrating in the in-plane flexural modes [27]. The prong length L is considerably larger than the prong width W and the thickness T. The prong cross-sectional area A along with the prong length L and the elastic modulus E are constants. The QTF prongs can be assumed to behave as two uncorrelated cantilevers [18]. According to

the Euler-Bernoulli approximation, a QTF vibrating in its in-plane flexural modes can be described by the fourth-order differential equation [28]:

$$E \cdot I \cdot \frac{\partial^4 y(x,t)}{\partial^4 x} + \rho \cdot A \cdot \frac{\partial^4 y(x,t)}{\partial^4 t} = 0 \quad (1)$$

where ρ is the density of the quartz, t is the time, x is the direction identified by the prong at its rest position and y is the direction orthogonal to x in the QTF plane, as shown in Fig. 1(b). The resonance frequency f_n can be obtained solving Eq. (1) by imposing boundary conditions at the supports of the cantilever prong:

$$f_n = \frac{\pi \cdot T}{8\sqrt{12}L^2} \cdot \sqrt{\frac{E}{\rho}} \cdot n^2 \quad (2)$$

where n=1.194 and n=2.988 for the fundamental flexural mode and the first overtone flexural mode, respectively. Using Eq. (2), a fundamental mode frequency of f_0 = 2,913 Hz and a 1st overtone mode of f_1 = 18,245 Hz were calculated. The parameter values used for the calculations are shown in Fig. 1(c).

2.2 Self-calibration principle of the CH_4 V-T relaxation

There are four normal modes of vibration for a CH_4 molecule: two symmetric vibrations ν_1 (stretching) and ν_4 (bending), and two asymmetric vibrations ν_2 (bending) and ν_3 (stretching). In the present work, the asymmetric stretching vibration ν_3 CH_4 band was selected and the related absorption line is located at 3038.5 cm^{-1}. To target this line, a distributed feedback (DFB) interband cascade laser (ICL) emitting at ~3.3 μm was implemented as the excitation light source. Though no H_2O absorption lines falls in the ICL tuning range, the presence of water vapor in the gas sample affects the CH_4 QEPAS signal amplitude, since it modifies the energy relaxation rates of the CH_4

molecules. Indeed, water vapor has a high density of vibrational levels, which creates multiple options for absorbed energy transfer in collisions with CH_4 molecules and a ladder for subsequent efficient multistep relaxation. Thereby, water molecules enhance the CH_4 photoacoustic signal since they act as promoters of the energy relaxation via collision/de-excitation process with CH_4 molecules.

When wet N_2 is used as the carrier gas, the V-T relaxation process of CH_4 can be analyzed using a simple model in which only a one-stage collision between molecules is considered [22]. In this model, the obtained CH_4 $2f$ QEPAS signal amplitude $S(P_H)$ can be determined from Eq. (3):

$$S(P_H) = S_1 + S_2 = S_1\left[1 + (\frac{S_\infty}{S_0} - 1) / \sqrt{1 + \frac{(2\pi \cdot f \cdot \tau_0^H \cdot P_0)^2}{P_H^2}}\right] \quad (3)$$

where S_0 and S_∞ are the CH_4 signals obtained with dry N_2 and saturated water pressure, respectively. S_1 is the CH_4 signal generated by both CH_4/N_2 collisions and CH_4/CH_4 collisions, which are independent on the H_2O concentration, while S_2 represents the contribution to the CH_4 signal due to CH_4/H_2O collisions depending on the H_2O partial pressure P_H. $\tau_0^H \cdot P_0$ is a constant which describes the V-T relaxation rate due to CH_4/H_2O collisions. In case of the QEPAS technique, the modulation frequency f is usually $>10^4$ Hz.

Eq. (3) can be expressed as a linear equation when the H_2O partial pressure P_H is low:

$$S(P_H) \approx S_1 + (\frac{S_\infty}{S_0} - 1) \cdot \frac{S_1}{2\pi \cdot f \cdot \tau_0^H \cdot P_0} \cdot P_H \quad (4)$$

The slop k of $S(P_H)$ is:

$$k = (\frac{S_\infty}{S_0} - 1) \cdot \frac{S_1}{2\pi \cdot f \cdot \tau_0^{\mathrm{H}} \cdot P_0} \quad (5)$$

After we get the value of the $\tau_0^{\mathrm{H}} \cdot P_0$ via the measured slop k, S_1 can be expressed as a simple function of $S(P_{\mathrm{H}})$ and P_{H}. Once the values of the $S(P_{\mathrm{H}})$ and P_{H} are simultaneously measured via the QTF fundamental and fist overtone detection channels, the CH_4 V-T relaxation influence from the H_2O can be calibrated and the real CH_4 concentration can be retrieved.

3. Description of sensor system

A schematic of the QEPAS sensor for CH_4 detection with V-T relaxation self-calibration is depicted in Fig. 2. A custom made QTF with a 17 mm prong length was implemented as the photoacoustic transducer. In a first step, a complete QTF response profile was measured to retrieve the resonance frequency of the custom QTF. A sine wave excitation signal was applied to one of the two QTF electrodes and the piezoelectric signals produced by the excited vibration were detected from the other QTF electrode when the frequency of the exciting signal was scanned. The peak of the QTF frequency response profile corresponds to the resonance frequency. The obtained experimental results were f_0 = 2,868 Hz and f_1 = 17,741 Hz, in good agreement with the expected values. The slight discrepancies between the experimental and theoretical QTF resonance frequencies are due to: (i) damping of the gas, (ii) variation of the cantilever density caused by the electrode gold layers, (iii) dependence of the quartz elasticity modulus on the crystallographic axes orientation, (iv) deviations between the modelled and the real QTF geometry. Previous experiments show that the largest QEPAS signal was obtained when the excitation

beam was positioned at 2.0 mm below the QTF opening for fundamental flexural vibration, while the excitation beam should be located at 9.5 mm below the QTF opening to ensure the most efficient prongs excitation when operating at the first overtone flexural frequency [24]. The large separation (7.5 mm) between the positions of the antinodes providing the maximum vibration amplitudes for the fundamental and the fist overtone mode, allows the parallel placement of two laser beams that can excite selectively the vibrational modes and act as two independent detection channels, thereby realizing a simultaneous dual-gas detection.

The first overtone detection channel possesses a higher sensitivity than the fundamental detection channel due to the QTF design, and hence the first overtone detection channel was used to detect the trace CH_4. A single-tube acoustic micro-resonator (AmR) with 0.62 mm inner diameter, 14.5 mm length and two 90 μm slits in the middle of the tube was positioned between two prongs of the QTF to enhance the first overtone QEPAS signal [29]. No AmR was equipped for the fundamental vibration mode as the 3 kHz fundamental resonance frequency requires a >100 mm AmR length [20], unfeasible for optical alignment. The QTF and AmR were enclosed inside a gas enclosure with two CaF_2 windows (not shown in Fig. 2), which constitutes an acoustic detection module (ADM).

A commercial gas dilution system (Environics, series 4000) was used and placed upstream to generate a CH_4 / H_2O / N_2 gas mixture at fixed concentrations. A valve was used to set the gas flow rate at 100 sccm. A mass flow meter (Alicat Scientific, Inc. Model M-2SLPM-D/5M) and a valve were placed upstream, while a pressure

controller (MKS Instruments Inc. Model 649B13TS1M22M) and a vacuum pump (KNF Technology Co., Ltd, N816.3KT.18) were placed downstream to monitor and controlled the pressure inside the sensor system.

A Nanoplus continuous wave DFB-ICL was used as the excitation source for the CH_4 detection. The laser can be operated in the temperature range of 10-25^{o}C with a temperature coefficient of -0.306 cm^{-1}/^{o}C and in the current range of 25-55 mA with a current coefficient of -0.095 cm^{-1}/mA. A CaF_2 lens with a focal length of 7.5 cm was used to focus the ICL beam into the ADM. A custom low noise current driver and a temperature controller (Thorlabs, Inc. Model TED200C) were equipped to drive the DFB-ICL. A near-infrared DFB laser (FITEL FRL15DCWD-A82), driven via an integrated driver board, was implemented for H_2O detection. The driver board set the wavenumber of the DFB laser at 7,306.75 cm^{-1} by controlling its temperature and current. To increase the sensitivity of the sensor, the 2*f*-WMS technique was used. A ramp signal and a sine wave signal with the frequency of $f_1/2$ were send to the custom current driver for CH_4 detection, while another ramp signal and a sine wave signal with the frequency of $f_0/2$ were send to the driver board for H_2O detection. All of the signal mentioned above were generated by a Labview controlled DAQ card (National Instrument, USB-6361). The signal output from the QTF was connected to a custom transimpedance amplifier with a feedback resistor of R_g= 10 MΩ and directed to the DAQ card. Two LabVIEW-based lock-in amplifiers (LIA#1 and LIA#2） were employed to demodulate the QEPAS signal at the frequency of $f_1/2$ and $f_0/2$ for CH_4 and H_2O detection, respectively. The detection bandwidth of the two LIAs was set at

0.833 Hz.

4. Optimization of the sensor performance

4.1 Gas absorption characteristics at 3,291 nm and 1,368 nm

The presence of H_2O not only affects the CH_4 QEPAS signal amplitude via acting as a promoter of V-T relaxation process, but also can interfere with the CH_4 spectrum profile if the selected target line is close to a H_2O absorption line with similar line strength [30, 31]. A CH_4 absorption line at 3038.5 cm^{-1} with a line intensity of 8.85 $\times 10^{-20}$ $cm \cdot mol^{-1}$ was selected as the target line based on the high-resolution transmission (HITRAN) 2012 molecular spectroscopic database [31]. Since the absorption intensities of the H_2O lines nearby the CH_4 target line are eight orders of magnitude smaller than that of the CH_4, interferences on the CH_4 QEPAS spectra profile from H_2O absorption is negligible. The H_2O absorption line located at 7,306.75 cm^{-1} with an intensity of 1.8 $\times 10^{-20}$ $cm \cdot mol^{-1}$ was selected as the H_2O target line [31]. The CH_4 lines nearby 7,306.75 cm^{-1} are three orders of magnitude smaller than the target H_2O line. As a result, no influence of the CH_4 on the H_2O detection has to be considered. In order to reach the target wavelength, the temperature of the DFB-ICL was set to 10 ^oC with an output power of 5.2 mW, while the temperature of near-infrared DFB laser was set to 16.4 ^oC with an output power of 11.3 mW.

4.2 Independence between the two different vibration modes

An experiment to check the independence between the fundamental and first overtone flexural vibration modes was carried out using a certified mixture of 500 ppm CH_4 in nitrogen (N_2) with 1.6% H_2O as the target gas. The target gas flowed

through the gas enclosure with a pressure of 200 Torr fixed by the pressure controller. To generate a specified H_2O mixing ratio, a certified mixture of 500 ppm CH_4 in N_2 was divided into two gas lines and directed to the gas dilution system to control the flow rate of the two gas lines, respectively. One gas line was humidified by the humidifier (Perm Select, PDMSXA-2500) and then mixed with another line at a selected flow rate ratio. The wavelengths of the DFB-ICL and near-infrared DFB laser were scanned in the period of 40 s and 120 s, which results in a scan rate of 0.023 cm^{-1}/s and 0.0067 cm^{-1}/s, respectively. The CH_4 QEPAS spectrum (purple line) measured from the first overtone channel and the H_2O QEPAS spectrum (blue line) measured from the fundamental channel were detected simultaneously and shown in Fig. 3(a) and Fig. 3(b), respectively. As shown in Fig. 3(a), the ADM with the single-tube AmR (purple line) provided a maximum signal amplitude of 18.3 mV, which is 45 times higher than that measured at the same condition but using the bare custom QTF (black line).

To verify the absence of any cross-talking between the two vibrational modes operation, in Fig. 3(a) are compared the two CH_4 QEPAS spectra measured using the first overtone detection channel when the QTF operated only at the overtone flexural mode (red circle symbols) and when both the fundamental and first overtone mode were simultaneously excited (purple line). The two CH_4 spectra overlap, confirming that the QTF fundamental and first overtone flexural modes did not interfere with each other, allowing simultaneous dual-gas detection.

4.3 Optimization of wavelength modulation depth and gas pressure

The 2*f* QEPAS signal amplitude is dependent on the wavelength modulation depth *A* and the gas pressure *P*. Thus, optimal *A* and *P* values must be found in order to obtain the highest QEPAS signal. A sample gas of 500 ppm CH_4 in N_2 with 1.6% H_2O was used to retrieve the optimal *A* and *P*. The data obtained from LIA#1 is shown in Fig. 4(a), corresponding to the CH_4 detection channel using the first overtone flexural mode. Fig. 4(b) shows the data measured from LIA#2, which is H_2O detection channel using the fundamental flexural mode. According to the experimental results, the highest value of the CH_4 QEPAS signals was recorded at *P* = 200 Torr, *A* = 4 mA, while the peak value of the H_2O QEPAS signals was achieved at P = 200 Torr, A = 8 mA. Hence, a pressure of 200 Torr with a 4 mA and 8 mA current modulation depths for DFB-ICL and near-infrared DFB laser were selected for the dual gas QEPAS sensor operation.

5. **Assessment of the sensor performance**

The response of the first overtone detection channel for various CH_4 concentrations with a fixed H_2O concentration at 1.6% is illustrated in Fig. 5(a). The CH_4 concentration was varied from 50 ppm to 500 ppm. The results were linearly fitted and the calculated R^2 value is 0.999 which confirms the linear response of the overtone detection channel with respect to the CH_4 concentration. A similar experiment was carried out to confirm the linearity to H_2O concentration of the fundamental detection channel. The response of the fundamental detection channel for various H_2O concentrations in a 500 ppm CH_4:N_2 mixtures is illustrated in Fig. 5(b). The R^2 value of 0.999 confirms the linearity of the fundamental channel.

As stated in section 2, water vapor in the $CH_4/H_2O/N_2$ gas sample mixture acts as a promoter of the CH_4 V-T relaxation. This is confirmed by the experimental results shown in Fig. 6, where the LD#1 wavelength was tuned to the center of the CH_4 absorption line and the overtone channel QEPAS signal amplitude measured for 500 ppm CH_4 concentration (black lines) is plotted as a function of water concentration in the mixtures, varying from 0% to 1.6%, corresponding to H_2O partial pressure P_H increasing from 0 to 6.4 Torr. The blue lines correspond to the correlated H_2O *2f* QEPAS signal amplitude, measured using the QTF fundamental channel. According to Eq. (4) and Eq. (5), the CH_4 QEPAS signal $S(P_H)$ can be linearly fitted as a function of P_H. And the slope k was obtained to be 0.00248 from the fitting. Hence, S_1 can be expressed as follow:

$$S_1 = \frac{S(P_H)}{1 + 0.9934 \cdot P_H} \tag{6}$$

To evaluate the self-calibration performance of the QEPAS sensor for CH_4 detection, a certified mixture of 500 ppm CH_4 in N_2 and water vapor were introduced into the sensor system. The H_2O concentration is varied in steps. The CH_4 QEPAS signal $S(P_H)$ (blue lines) and H_2O QEPAS signal P_H (black lines) were recorded as a function of time, as shown in Fig. 7(a). The calculated S_1 values (red line) are also depicted in Fig. 7(a). The stability of the S_1 value confirms the capability of the realized QEPAS sensor to normalize the influence of the H_2O molecules on the CH_4 V-T relaxation.

Furthermore, the QEPAS sensor shows very good performance in term of optical noise. Indeed, as shown in Fig. 7(b) and Fig. 7(c), the noise levels measured from the

fundamental and the first overtone detection channels are 1.72 μV and 1.9 μV, respectively, very similar to the estimated theoretical thermal noise of 1.6 μV. Based on the reported data, the minimum detection limits (1σ) at 1-s integration time and corresponding NNEA coefficients achieved are 50 ppb and 2.9×10^{-9} $cm^{-1}\cdot W/Hz^{1/2}$ for CH_4, and 32 ppm and 6.3×10^{-7} $cm^{-1}\cdot W/Hz^{1/2}$ for H_2O, respectively.

An Allan-Werle deviation analysis for the fundamental and first overtone detection channels was performed in pure N_2 to evaluate the long-term stability of the self-calibration QEPAS sensor. The results are shown in Fig. 8. The Allan-Werle deviation plots follows a $1/\sqrt{t}$ dependence for all time sequences, which indicates that the white Johnson noise of the QTF remains the dominant source for both detection channels and the sensor allows data averaging without a base line or sensitivity drift up to a 200 s time scale [32].

6. Atmospheric CH_4 measurement near the Hou village landfill

Hou Village Landfill (HVL), the largest sanitary landfill in Shanxi province, is located in the northeast of Taiyuan city with a service life of 17 year. More than ten million tons of MSW have accumulated in HVL since 2008, which means about 4×10^8 Nm^3 LFG is generated per year. Although vertical and horizontal gas wells are operated, the CH_4 emitted to the atmosphere with the LFG can not be ignored. To monitor the CH_4 levels in the atmosphere near the landfill, continuous CH_4 field measurements were carried out near the HVL on October 11, 2018. The QEPAS based CH_4 sensor with V-T relaxation self-calibration was mounted in a car and power was supplied by the car battery with the help of an AC inverter (Wagan Tech, 9622). The

demodulation of the CH_4 QEPAS signal and H_2O QEPAS signal，the data acquisition of the 2*f* signal amplitude via a Levenberg-Marquardt nonlinear least-squares fit procedure, as well as the calibration of the CH_4 V-T relaxation were carried out using a dedicated LabVIEW-based program. The data updating rate of the program was set to 10 s. These measurements were performed for 3 hours, from 10:30 am to 13:30 pm, as shown in Fig. 9.

The average atmospheric CH_4 concentration measured near the HVL resulted in ~ 2.9 ppm, 50% more than the mean value in atmosphere (1.8 ppm). The observed three CH_4 plumes with peak values of ~ 4.1 ppm, 4.3 ppm and 5.9 ppm were generated by the wind blowing from the direction of the LFG collection system. The periodic sharp peaks, with ~ 45 min interval time, were generated by MSW truck passing near the CH_4 sensor. During all the measurements the H_2O concentration remains below 1.6 %

7. Conclusions

In summary, a CH_4 QEPAS sensor with V-T relaxation self-calibration was developed based on the in-plane fundamental and 1st overtone vibration simultaneous operation of a custom QTF. The 7.5 mm separation between the positions of the two antinodes for two different vibration modes permits accommodating two laser beams to implement the FDM detection of the QTF signals, thus realizing dual-gas QEPAS sensor. The fundamental vibrational channel was used for H_2O detection, while the first overtone vibrational channel was employed to monitor CH_4. A theoretical model of V-T relaxation and self-calibration method were developed to normalize the

influence of H_2O molecule on the CH_4 V-T energy relaxation rate. The measured value of the NNEA of 2.9×10^{-9} $cm^{-1}\cdot W/Hz^{1/2}$ for CH_4 detection is similar to previously reported results on QEPAS-based CH_4 detection systems but the influences of H_2O on the CH_4 V-T relaxation was removed. Continuous monitoring of atmospheric CH_4 near the largest waste landfill in Shanxi Province was performed to demonstrate the capability of the reported sensor system for in-situ measurements. Possible future applications for the developed dual gas sensing method are: non-invasive breath analysis diagnostics in which H_2O concentration of > 4% can be reached, measurement of isotopes abundance ratio (like $^{12}CH_4/^{13}CH_4$ or $^{12}CO_2/^{13}CO_2$) and chemical reaction control where the two-detection channel could be employed to monitor the composition ratio of two chemical reacting species.

Acknowledgements

This material is based upon work supported by National Key Research and Development Program of China (No. 2017YFA0304203); National Natural Science Foundation of China (Grants #61622503, 61805132, 61575113, 11434007); Scientific Research Foundation (No. 227545028); Changjiang Scholars and Innovative Research Team in University of Ministry of Education of China (No. IRT_17R70); 111 project (Grant No. D18001), Outstanding Innovative Teams of Higher Learning Institutions of Shanxi; Shanxi “1331 Project” key subjects construction; Applied basic research program of Shanxi province (No. 201801D221174). Financial support from THORLABS GmbH, within the joint-research laboratory PolySense is acknowledge.

References

[1] W. Ren, W. Jiang, F. K. Tittel, Single-QCL-based absorption sensor for simultaneous trace-gas detection of CH_4 and N_2O, Appl. Phys. B 117 (2014) 245-251.

[2] K. Liu, L.Wang, T. Tan, G. Wang, W. Zhang, W. Chen, X. Gao, Highly sensitive detection of methane by near-infrared laser absorption spectroscopy using a compact dense-pattern multipass cell, Sens. Actuators B: Chem. 220 (2015) 1000-1005.

[3] E. F. Aghdam, C. Scheutz, P. Kjeldsen, Impact of meteorological parameters on extracted landfill gas composition and flow, Waste Manage, https://doi.org/10.1016/j.wasman.2018.01.045.

[4] C. Yaman, Y. Küçükağa, B. Pala, G. Delice, N. E. Korkut, A. Akyol, S. Kara, Enhancement of landfill gas production and waste stabilisation by using geotextile filter in a bioreactor landfill, Int. J. Global Warming, https://doi.org/ 10.1504/IJGW.2019.096757.

[5] M. W. Sigrist, Trace gas monitoring by laser photoacoustic spectroscopy and related techniques, Rev. Sci. Instrum. 74 (2003) 486-490.

[6] L. Dong, F.K. Tittel, C. Li, N.P. Sanchez, H. Wu, C. Zheng, Y. Yu, A. Sampaolo, R.J. Griffin, Compact TDLAS based sensor design using interband cascade lasers for mid-IR trace gas sensing, Opt. Express 24 (2016) A528.

[7] C. Zheng, W. Ye, N.P. Sanchez, A.K. Gluszek, A.J. Hudzikowski, C. Li, L. Dong, R. J. Griffin, F.K. Tittel, Infrared dual-gas CH_4/C_2H_6 sensor using two continuouswave interband cascade lasers, IEEE Photonics Technol. Lett. 28 (2016) 2351.

[8] L. Hu, C. Zheng, D. Yao, D. Yu, Z. Liu, J. Zheng, Y. Wang, F. K. Tittel, A hollow-core photonic band-gap fiber based methane sensor system capable of reduced mode interference noise, Infrared Phys. Techn. 97 (2019) 101-107.

[9] C. Massie, G. Stewart, G. McGregor, J. R. Gilchrist, Design of a portable optical sensor for methane gas detection, Sens. Actuators B: Chem. 113 (2006) 830-836.

[10] C. Zheng, W. Ye, N. P. Sanchez, C. Li, L. Dong, Y. Wang, R. J. Griffin, F. K. Tittel, Development and field deployment of a mid-infrared methane sensor without pressure control using interband cascade laser absorption spectroscopy, Sens. Actuators B: Chem. 244 (2017) 365-372.

[11] P. Patimisco, A. Sampaolo, L. Dong, F. K. Tittel, V. Spagnolo, Recent advances in quartz enhanced photoacoustic sensing, App. Phys. Rev. 5 (2018) 011106.

[12] L. Dong, J. Wright, B. Peters, B. A. Ferguson, F. K. Tittel, S. McWhorter, Compact QEPAS sensor for trace methane and ammonia detection in impure hydrogen, Appl. Phys. B 107 (2012) 459-467.

[13] A. Sampaolo, S. Csutak, P. Patimisco, M. Giglio, G. Menduni, V. Passaro, F. K. Tittel, M. Deffenbaugh, V. Spagnolo, Methane, ethane and propane detection using a compact quartz enhanced photoacoustic sensors and a single interband cascade laser, Sens. Actuators B: Chem. 282 (2019) 952-960.

[14] M. Jahjah, W. Kiang, N.P. Sanchez, W. Ren, P. Patimisco, V. Spagnolo, S. C. Herndon, R. J. Griffin, F. K. Tittel, Atmospheric CH_4 and N_2O measurements near Greater Houston area landfills using QCL-based QEPAS sensor system during DISCOVERY-AQ 2013, Opt. Lett. 39 (2014) 957.

[15] Z. Wang, Q. Wang, J. Y. Ching, J. C. Wu, G. Zhang, W. Ren, A portable low-power QEPAS-based CO_2 isotope sensor using a fiber-coupled interband cascade laser, Sens. Actuators B: Chem. 246 (2017) 710-715.

[16] Z. Li, Z. Wang, Y. Qi, W. Jin, W. Ren, Improved evanescent-wave quartz-enhanced photoacoustic CO sensor using an optical fiber taper, Sens. Actuators B: Chem. 248 (2017) 1023-1028.

[17] M. Mordmueller, M. Koehring, W. Schade, U. Willer, An electrically and optically cooperated QEPAS device for highly integrated gas sensors, Appl. Phys. B 119 (2015) 111-118.

[18] P. Patimisco, A. Sampaolo, L. Dong, M. Giglio, G. Scamarcio, F. K. Tittel, and V. Spagnolo, Analysis of the electro-elastic properties of custom quartz tuning forks for optoacoustic gas sensing, Sens. Actuators B: Chem. 227 (2016) 539-546.

[19] P. Patimisco, A. Sampaolo, M. Giglio, S. Dello Russo, V. Mackowiak, H. Rossmadl, A. Cable, F.K. Tittel, V. Spagnolo, Tuning forks with optimized geometries for quartz-enhanced photoacoustic spectroscopy, Opt. Express 27, (2019) 1401-1415.

[20] L. Dong, A. A. Kosterev, D. Thomazy, F. K. Tittel, QEPAS spectrophones: design, optimization and performance, Appl. Phys. B 100 (2010) 627-635.

[21] Y. Ma, Y. He, X. Yu, C. Chen, R. Sun, F. K. Tittel, HCl ppb-level detection based on QEPAS sensor using a low resonance frequency quartz tuning fork, Sens. Actuators B: Chem. 233 (2016) 388-393.

[22] X. Yin, L. Dong, H. Zheng, X. Liu, H. Wu, Y. Yang, W. Ma, L. Zhang, W. Yin, L. Xiao, S. Jia, Impact of humidity on quartz-enhanced photoacoustic spectroscopy

based CO detection using a near-ir telecommunication diode laser, Sensors 16 (2016) 16020162.

[23] J. Li, U. Parchatka, H. Fischer, Development of field-deployable QCL sensor for simultaneous detection of ambient N_2O and CO, Sens. Actuators B: Chem. 182 (2013) 659-667.

[24] A. Sampaolo, P. Patimisco, L. Dong, A. Geras, G. Scamarcio, T. Starecki, F. K. Tittel, and V. Spagnolo, Quartz-enhanced photoacoustic spectroscopy exploiting tuning fork overtone modes, Appl. Phys. Lett. 107 (2015) 231102.

[25] K. Waszczuk, T. Piasecki, K. Nitsch, T. Gotszalk, Application of piezoelectric tuning forks in liquid viscosity and density measurements, Sens. Actuators B: Chem. 160 (2011) 517-523.

[26] H. Wu, L. Dong, W. Ren, W. Yin, W. Ma, L. Zhang, S. Jia, F. K. Tittel, Position effects of acoustic micro-resonator in quartz enhanced photoacoustic spectroscopy, Sens. Actuators B: Chem. 206 (2015) 364–370.

[27] F. K. Tittel, A. Sampaolo, P. Patimisco, L. Dong, A. Geras, T. Starecki, V. Spagnolo, Analysis of overtone flexural modes operation in quartz-enhanced photoacoustic spectroscopy, Opt. Express 24 (2016) A682-A692.

[28] M. Christen, Air and gas damping of quartz tuning forks, Sens. Actuators A: Phys 4 (1983) 555-564.

[29] H. Zheng, L. Dong, A. Sampaolo, P. Patimisco, W. Ma, L. Zhang, W. Yin, L. Xiao, V. Spagnolo, S. Jia, F. K. Tittel, Overtone resonance enhanced single-tube on-beam quartz enhanced photoacoustic spectrophone, Appl. Phys. Lett. 109 (2016)

111103.

[30] J. Li, H. Deng, J. Sun, B. Yu, H. Fischer, Simultaneous atmospheric CO, N_2O and H_2O detection using a single quantum cascade laser sensor based on dual-spectroscopy techniques, Sens. Actuators B: Chem. 231 (2016) 723-732.

[31] Hitran database. Available from: http://www.hitran.org/

[32] M. Giglio, P. Patimisco, A. Sampaolo, G. Scamarcio, F. K. Tittel and V. Spagnolo, Allan Deviation Plot as a Tool for Quartz Enhanced Photoacoustic Sensors Noise Analysis, IEEE Trans. Ultr. Freq. Contr. 63 (2016) 555-560.

Figure captions:

Fig. 1 (a) Electrical model of a custom QTF operating simultaneously at the fundamental (area inside the red dotted rectangle) and 1st overtone in-plane vibrational modes (area inside the blue dotted rectangle). C_p is the parallel stray capacitance of the *RLC* components. (b) Schematic of the deformation (not in scale) of the QTF prongs in the combined vibration at the fundamental and overtone vibration modes. The black imaginary line and the gold line in Fig. 1(b) represent the QTF prong deformation when the QTF is vibrating in the fundamental and first overtone flexural modes, respectively. (c) Dimensions and parameters of the custom QTF. *L*: QTF prong length, *T*: thickness of the prong, *E*: elastic modulus for the quartz, ρ: the density of the quartz.

Fig. 2 Schematic of the CH_4 QEPAS sensor with V-T relaxation self-calibration. Rg: the feedback resistor of a custom made transimpedance amplifier, DAQ card: data acquisition card.

Fig. 3 (a) QEPAS spectra of 500 ppm CH_4 in nitrogen (N_2) with 1.6% H_2O detected with the QTF plus single tube micro-resonator using only the 1st overtone detection channel (red dots) or when operating with both the fundamental and 1st overtone modes (violet curves). The black curve is the QEPAS spectrum acquired with the bare QTF using only the 1st overtone detection channel. (b) 1.6% H_2O spectra measured using the fundamental detection channel with the QTF operating also with the 1st overtone vibrational excitation. All QEPAS spectra were measured at a gas pressure of 200 Torr.

Fig. 4 2*f* QEPAS peak signal of H_2O (a) and CH_4 (b) QEPAS spectra measured at different gas pressures and laser current modulation depths. All measurements were performed using a 500 ppm CH_4 mixture in N_2 and 1.6% H_2O.

Fig. 5 The CH_4 and H_2O QEPAS signals obtained from the 1st overtone and the fundamental detection channels of the custom QTF, respectively, when the QTF is operating simultaneously in both modes.

Fig. 6 CH_4 QEPAS peak signal of a 500 ppm CH_4/N_2 mixture as a function of H_2O concentration. The H_2O concentration was varied from 0 to 1.6%, corresponding to variation of partial pressure P_H from 0 to 6.4 Torr.

Fig.7 (a) CH_4 QEPAS peak signal (blue lines) recorded as a function of time with the H_2O concentration varying in steps. H_2O QEPAS peak signal (black lines) recorded as a function of time with the H_2O concentration varying in steps. The red lines show the calculated S_1 values according to Eq. (6). **(b)** and **(c)** Enlarged views of the H_2O and CH_4 QEPAS signals used for the noise level analysis of the fundamental and first overtone detection channels, respectively.

Fig. 8 Allan-Werle deviations as a function of the data averaging period measured for pure N_2 gas samples. Red solid line: DFB-ICL wavelength was locked to the CH_4 absorption line at 3038.5 cm^{-1}. Blue solid line: near-infrared laser wavelength was locked to the H_2O absorption line at 7306.75 cm^{-1}. Dashed lines: $1/\sqrt{t}$ slope.

Fig. 9 Continuous atmospheric CH_4 measurement near the Hou Village Landfill, Taiyuan, China on Oct. 11, 2018.

Fig. 1

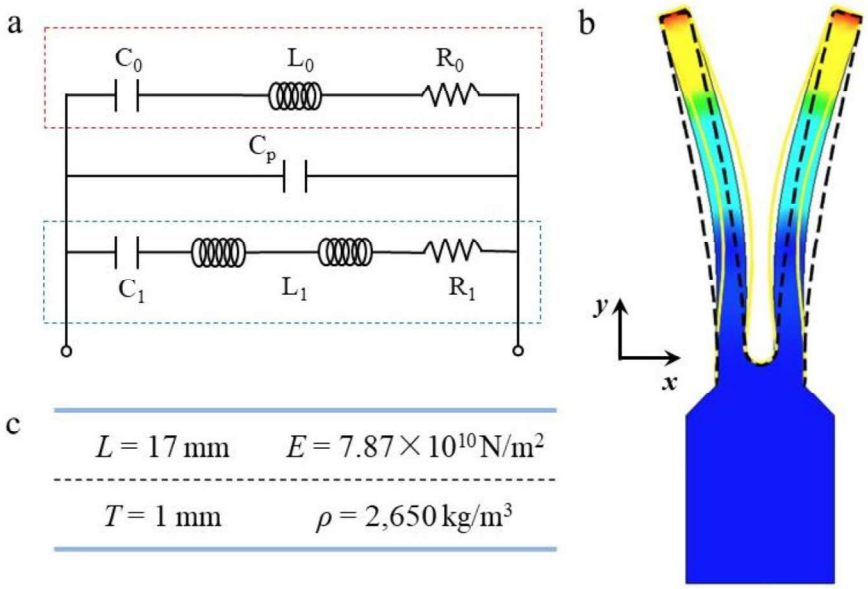

Fig. 2

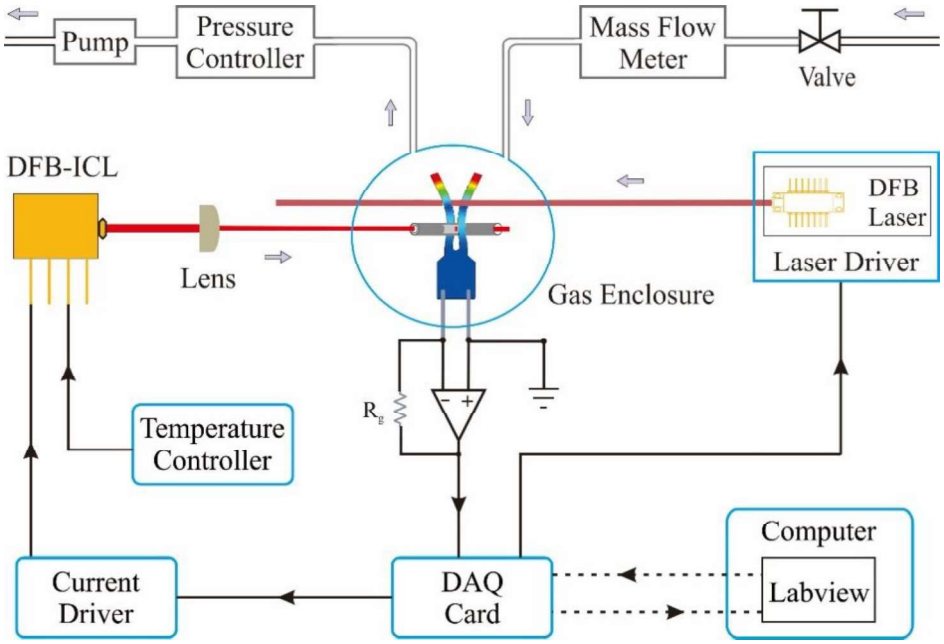
Pump
Pressure Controller
Mass Flow Meter
Valve
DFB-ICL
Lens
Gas Enclosure
DFB Laser
Laser Driver
R_g
Temperature Controller
Computer
Labview
Current Driver
DAQ Card

Fig. 3

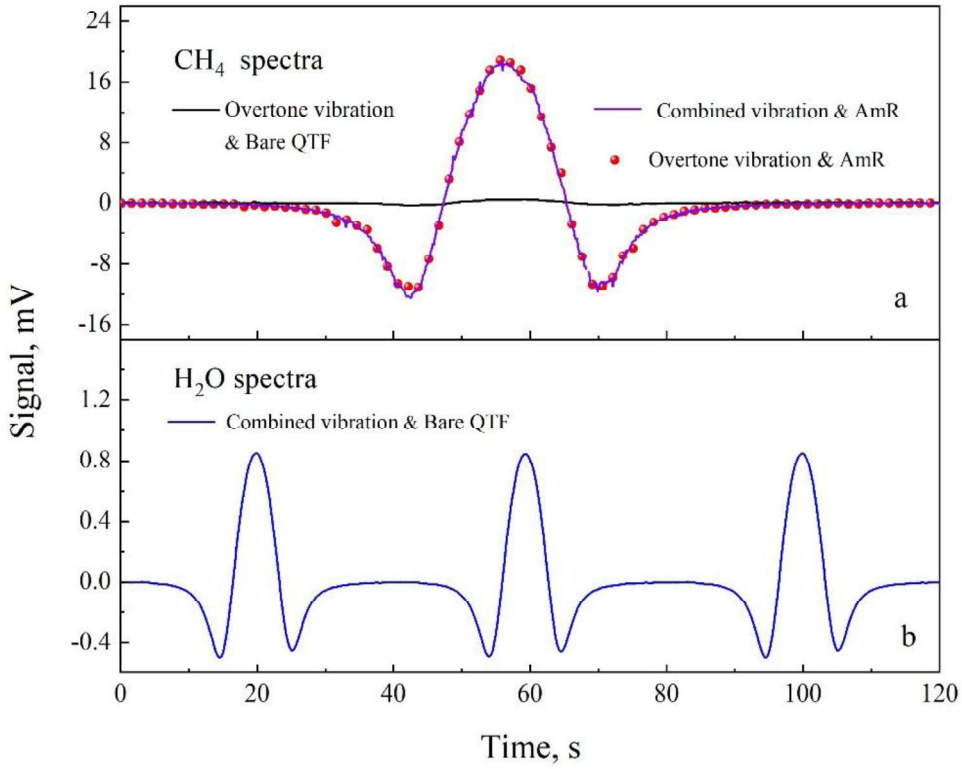
CH4 spectra
Overtone vibration & Bare QTF
Combined vibration & AmR
Overtone vibration & AmR
a
H2O spectra
Combined vibration & Bare QTF
b
Signal, mV
Time, s
24
16
8
0
-8
-16
1.2
0.8
0.4
0.0
-0.4
0
20
40
60
80
100
120

Fig. 4

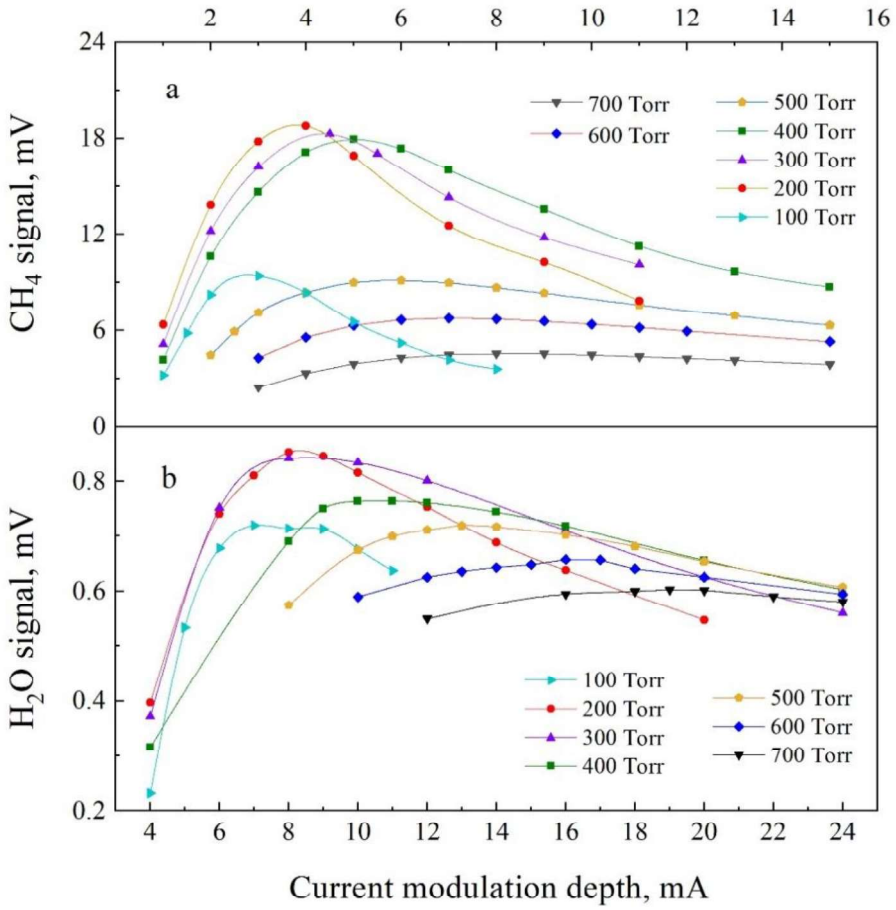
a
b
CH_4 signal, mV
H_2O signal, mV
Current modulation depth, mA
700 Torr
600 Torr
500 Torr
400 Torr
300 Torr
200 Torr
100 Torr

Fig. 5

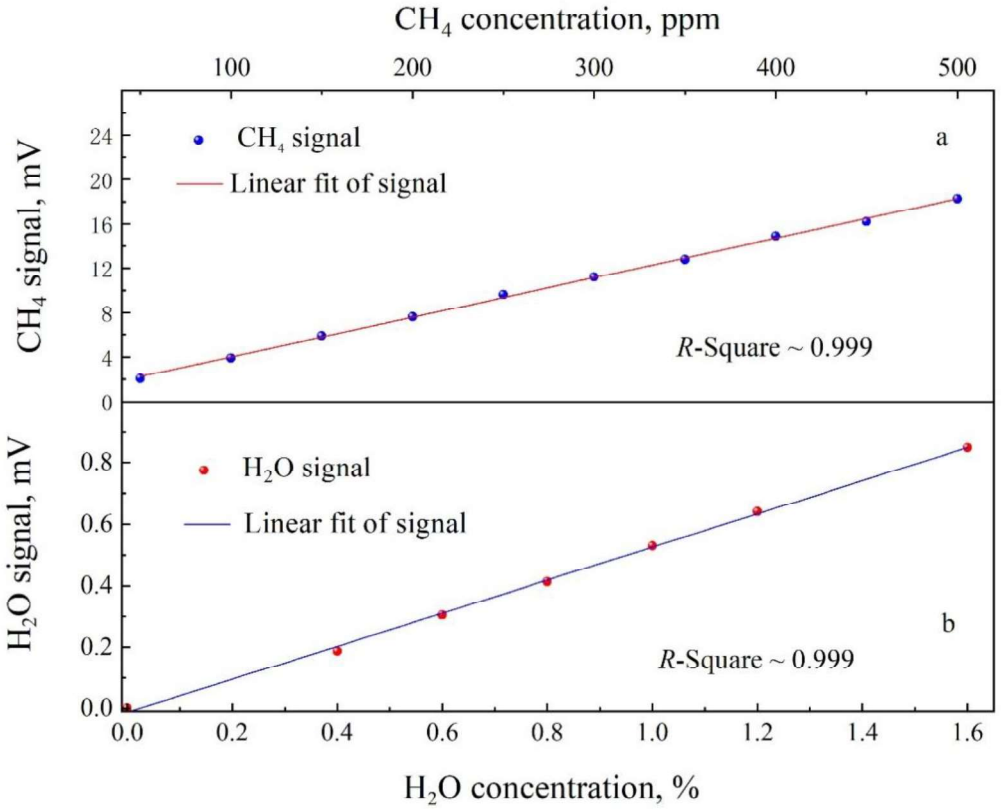
CH4 concentration, ppm
100
200
300
400
500
CH4 signal, mV
CH4 signal
Linear fit of signal
a
R-Square ~ 0.999
H2O signal, mV
H2O signal
Linear fit of signal
b
R-Square ~ 0.999
H2O concentration, %

Fig. 6

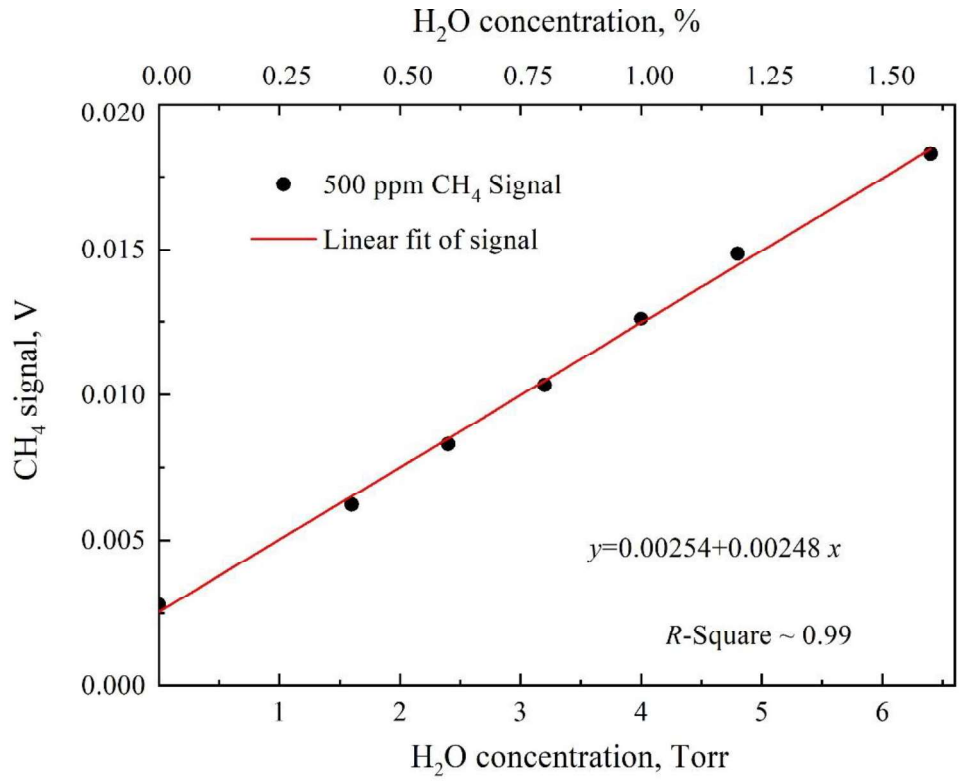
H2O concentration, %
0.00
0.25
0.50
0.75
1.00
1.25
1.50
0.020
0.015
0.010
0.005
0.000
CH4 signal, V
500 ppm CH4 Signal
Linear fit of signal
y=0.00254+0.00248 x
R-Square ~ 0.99
1
2
3
4
5
6
H2O concentration, Torr

Fig. 7

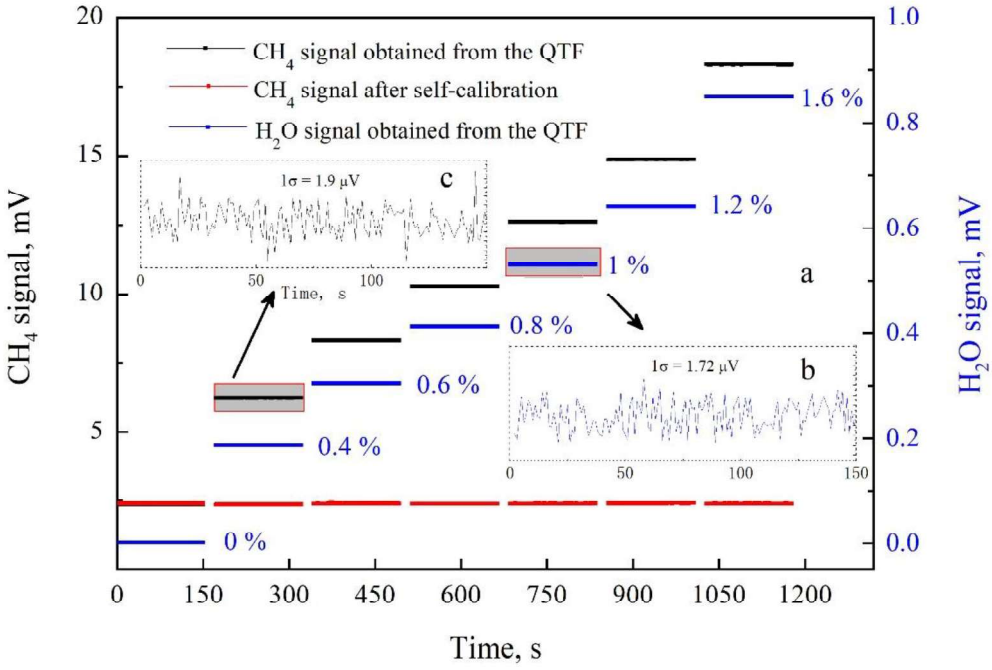
CH4 signal obtained from the QTF
CH4 signal after self-calibration
H2O signal obtained from the QTF
1σ = 1.9 μV
c
Time, s
1σ = 1.72 μV
b
a
0 %
0.4 %
0.6 %
0.8 %
1 %
1.2 %
1.6 %
CH4 signal, mV
H2O signal, mV
Time, s

Fig. 8

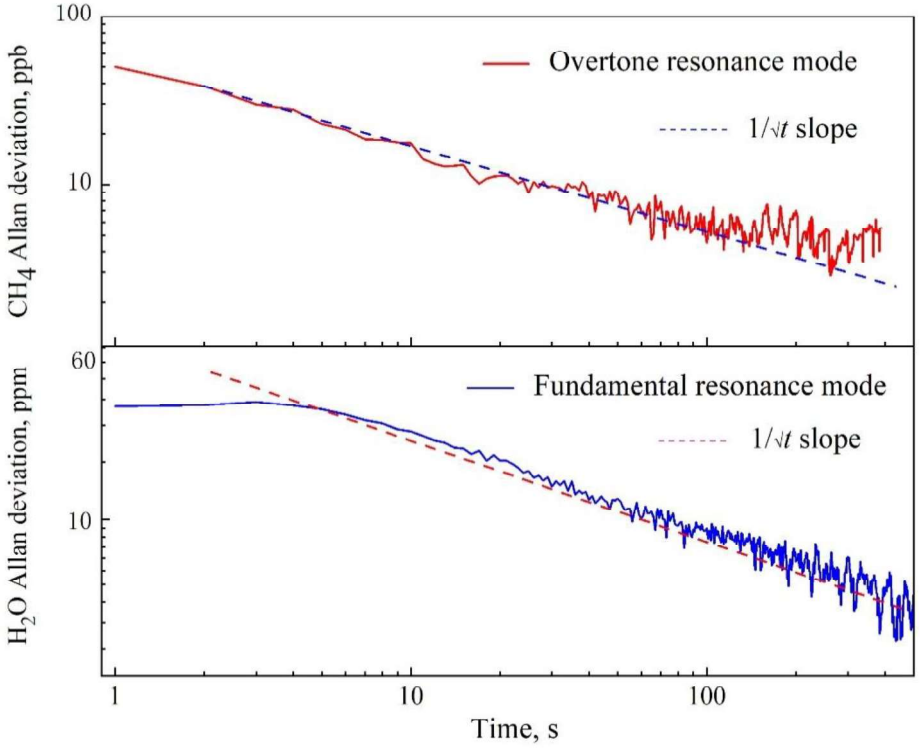
100
10
CH_4 Allan deviation, ppb
Overtone resonance mode
1/√t slope
60
10
H_2O Allan deviation, ppm
Fundamental resonance mode
1/√t slope
1
10
100
Time, s

Fig. 9

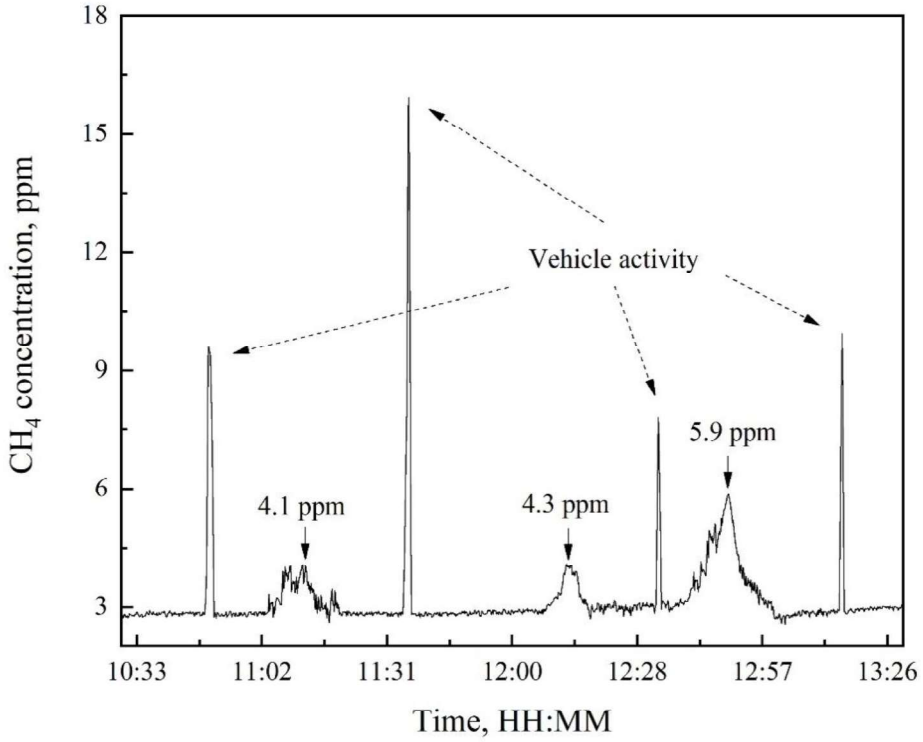
18
15
12
9
6
3
CH4 concentration, ppm
Vehicle activity
4.1 ppm
4.3 ppm
5.9 ppm
10:33
11:02
11:31
12:00
12:28
12:57
13:26
Time, HH:MM